GEOPHYSICS, VOL. 79, NO. 1 (JANUARY-FEBRUARY 2014); P. T27–T35, 7 FIGS., 1 TABLE.
10.1190/GEO2013-0093.1

Krauklis wave initiation in fluid-filled fractures by seismic body waves

Marcel Frehner[1]

ABSTRACT

Krauklis waves are a special wave mode that is bound to and propagates along fluid-filled fractures. They can repeatedly propagate back and forth along a fracture and eventually fall into resonance emitting a seismic signal with a dominant characteristic frequency. They are of great interest because this resonant behavior can lead to strongly frequency-dependent propagation effects for seismic body waves and may explain seismic tremor generation in volcanic areas or affect microseismic signals in fractured fluid reservoirs. It has been demonstrated that Krauklis waves can be initiated by a seismic source inside the fracture, for example by hydrofracturing. Here, the aim is to study Krauklis wave initiation by an incident plane P- or S-wave in numerical simulations. Both seismic body waves are reflected and scattered at the fracture, but also, two Krauklis waves are initiated with significant amplitude, one at each fracture tip (i.e., at the diffraction-points of the fracture). Generally, the incident S-wave initiates larger-amplitude Krauklis waves compared to the incident P-wave case. For both incident wave modes, the initiation of Krauklis waves strongly depends on the fracture orientation. In the case of an incident P-wave, large-amplitude Krauklis waves are initiated at moderate (12°–40°) and high (>65°) inclination angles of the fracture with a distinct gap at approximately 50°. The dependency of Krauklis wave initiation on fracture orientation is almost inversed in the case of an incident S-wave and the largest-amplitude Krauklis waves are initiated at an S-wave incidence angle of approximately 50°. The initiation of large-amplitude Krauklis waves by both P- and S-waves has important implications for earthquake signals propagating through fluid-bearing fractured rocks (volcanic areas, fluid-reservoirs) or for seismic exploration surveys in fractured reservoir situations.

INTRODUCTION

The presence of fluids in reservoir rocks has a major effect on seismic wave propagation behavior; for example, dispersion and frequency-dependent attenuation (Biot, 1962; White, 1975; Bourbie et al., 1987; Carcione, 2001; Quintal et al., 2011). Research on fluid-related seismic effects faces some scientific challenges and is significant for various industrial applications. One particular challenge is the interaction of simultaneous physical processes on different length scales. Because not all scales can be modeled at once, microscale processes have to be upscaled and their macroscale effects are described in effective medium models (e.g., Lambert et al., 2013). For the case of porous rocks such as sandstone, this is done successfully, for example in the Biot theory (Biot, 1962), the squirt-flow theory (Mavko and Jizba, 1991; Dvorkin et al., 1995), or the patchy-saturation model (White, 1975; White et al., 1975).

Despite including many effects in porous rocks, existing effective medium models have more difficulties describing fracture-related phenomena. One such phenomenon of particular interest is the so-called Krauklis wave, which is a special wave mode that is bound to and propagates along fluid-filled fractures. They are highly dispersive with a very low-phase velocity at low frequencies (Ferrazzini and Aki, 1987; Ashour, 2000; Korneev, 2008). There has been some confusion about the terminology because they have been referred to as *Krauklis waves* in Korneev (2011) and Frehner (2013), *Stoneley-guided waves* in Korneev et al. (2009), Frehner and Schmalholz (2010), and Korneev (2010), *crack waves* in Chouet (1986) and Yamamoto and Kawakatsu (2008), *slow Stoneley waves* in Ferrazzini and Aki (1987), or *Stoneley waves in a fracture* in Ashour (2000). Strictly speaking, a Stoneley wave is an interface wave propagating along an interface between two solid (elastic) half-spaces (Stoneley, 1924) and a Scholte wave is an interface wave propagating along an interface between a solid (elastic)

Manuscript received by the Editor 6 March 2013; revised manuscript received 22 August 2013; published online 6 December 2013.
[1]ETH Zurich, Geological Institute, Zurich, Switzerland. E-mail: marcel.frehner@erdw.ethz.ch.

and a fluid (viscous) half-space (Scholte, 1942a, 1942b). On the other hand, a Krauklis wave is a guided wave propagating along a fluid-filled fracture. In other words, a Krauklis wave is the interference between two Scholte waves (one along each fracture wall) propagating very close together. This also explains the high-frequency limit of the Krauklis wave phase velocity, which approaches the Scholte wave phase velocity when the wavelength is much smaller than the fracture thickness (Carcione and Helle, 2004). Krauklis (1962), Lloyd and Redwood (1965), and Paillet and White (1982) are among the first to study Krauklis waves. After Maksimov et al. (2011) and Korneev (2011) already used this terminology, several active researchers in this area have recently suggested (Korneev et al., 2012) to consistently name this wave mode the Krauklis wave, after its first investigator.

Krauklis waves are of great interest because they may fall into resonance and emit a seismic signal with a characteristic frequency. Because they are reflected at the fracture tip (Frehner and Schmalholz, 2010), they may propagate back and forth along a fracture of finite length. This resonance effect was used by Aki et al. (1977) and Chouet (1988, 1996) to explain long-period volcanic tremors recorded prior to volcanic eruptions, which can potentially be used for eruption forecasting. The Krauklis waves themselves cannot be detected at a relatively short distance from the fracture due to the spatially exponential decay of their amplitude (Ferrazzini and Aki, 1987). However, Frehner and Schmalholz (2010) investigated the reflection process of Krauklis waves at the tip of a fracture. They find that a part of the Krauklis wave is reflected and a part is scattered at the fracture tip and seismic body waves are radiated into the surrounding rock. This radiation eventually makes the detection of Krauklis wave-related signals (i.e., the tremor signal) possible.

Similar to volcanic areas, Krauklis waves may be of great importance in any other fluid-bearing rock containing fractures, for example, in fractured hydrocarbon reservoirs, geothermal systems, or for CO_2-sequestration in subsurface reservoirs, where they may be responsible for generating nonvolcanic seismic tremor signals. In particular, Krauklis waves are relevant for hydrofracturing and microseismicity applications. Fracture opening events triggered by fluid overpressure (i.e., hydrofracturing; Ferrazzini et al., 1990) represent a seismic source inside the fracture, which can initiate Krauklis waves with particularly high amplitude (Chouet, 1986; Frehner and Schmalholz, 2010). Therefore, Ferrazzini et al. (1990), Groenenboom and Falk (2000), and Groenenboom and van Dam (2000) used Krauklis waves for monitoring hydrofracturing.

The dispersion behavior of Krauklis waves is described in detail by various analytical studies (Ferrazzini and Aki, 1987; Ashour, 2000; Korneev, 2008, 2010, 2011) but only for simple geometries (infinitely long fractures with straight walls or a layered medium in the case of Korneev, 2011). At the same time, the few existing numerical studies (Chouet, 1986; Yamamoto and Kawakatsu, 2008; Frehner and Schmalholz, 2010) also do not include complex geometries. Common to all of these studies is that they assume that a Krauklis wave is initiated within the fracture, for example, by a fracture opening event due to hydrofracturing. However, it remains unstudied if Krauklis waves can be initiated by a body wave passing a fluid-filled fracture. Korneev (2008) speculates that the initiation of Krauklis waves by an incident body wave "should lead to strongly frequency dependent propagation effects for seismic waves" and Korneev et al. (2009) adds: "It is likely that Stoneley guided wave [i.e., Krauklis wave] is a key phenomenon which might explain observed frequency-dependent and nonlinear behavior of fluid reservoirs." Such behavior has major implications, for example, for earthquake signals propagating through fluid-bearing fractured rocks (e.g., volcanic areas, fluid reservoirs) or for active seismic surveys in hydrocarbon or geothermal reservoir applications. Korneev (2010) emphasizes "the importance of including these wave effects into poroelastic theories" and Frehner and Schmalholz (2010) predict that "future studies will help to include SGW [i.e., Krauklis wave]-related effects into more realistic models for fractured rocks."

Whether or not, and with which amplitude, Krauklis waves can be initiated by body waves is the main scope of the presented work. Previous analytical and numerical studies by Derov et al. (2008) and Maksimov et al. (2011) suggest that such an initiation is possible. Yet, these studies had several limitations: (1) a peculiar model geometry with a ring-shaped fracture and a source on the symmetry axis had to be chosen due to the used cylindrical symmetry, (2) a pressure point source was used emitting only P-waves, (3) the point source was in a finite distance allowing neither for a true incident plane wave nor for an incident angle of 0°, (4) rectangular fracture edges were used to ease the finite-difference calculation using a rectangular grid, and (5) an inviscid fluid was used. The present study extends and generalizes the previous learning from Derov et al. (2008) and Maksimov et al. (2011), as well as from Frehner (2013), by using true plane P- and S-waves as a seismic source and by using a more natural model consisting of a single water-filled (viscous) fracture with smooth (elliptical) fracture tips and any orientation with respect to the incident wave. In addition, the initiated Krauklis wave amplitudes are quantified as a function of the incident wave mode (P- or S-wave) and incident angle.

NUMERICAL METHOD AND SETUP

Krauklis waves are a truly multiscale phenomenon. The fracture thickness, the wavelength of the Krauklis wave or of seismic body waves, and the size of the fractured reservoir correspond to three length scales with entirely different orders of magnitude. For numerical simulations, this "presents a major computational challenge" (Korneev, 2008). However, Frehner and Schmalholz (2010) presented a finite-element (FE) study demonstrating the capability of numerical simulations to deal with this multiscale challenge. The same FE method as in Frehner et al. (2008) and Frehner and Schmalholz (2010) is adapted here to study the initiation of Krauklis waves by a passing body wave and is only briefly summarized here. The employed FE algorithm solves the viscoelastic wave equation in two dimensions:

$$\rho \begin{Bmatrix} \ddot{u}_x \\ \ddot{u}_y \end{Bmatrix} = \begin{bmatrix} \partial/\partial x & 0 & \partial/\partial y \\ 0 & \partial/\partial y & \partial/\partial x \end{bmatrix} \begin{Bmatrix} \sigma_{xx} \\ \sigma_{yy} \\ \sigma_{xy} \end{Bmatrix}, \tag{1}$$

$$\begin{Bmatrix} \sigma_{xx} \\ \sigma_{yy} \\ \sigma_{xy} \end{Bmatrix} = \begin{bmatrix} K+\frac{4}{3}\mu & K-\frac{2}{3}\mu & 0 \\ K-\frac{2}{3}\mu & K+\frac{4}{3}\mu & 0 \\ 0 & 0 & \mu \end{bmatrix} \begin{Bmatrix} \partial u_x/\partial x \\ \partial u_y/\partial y \\ \frac{\partial u_x}{\partial y}+\frac{\partial u_y}{\partial x} \end{Bmatrix} + \begin{bmatrix} \frac{4}{3}\eta & -\frac{2}{3}\eta & 0 \\ -\frac{2}{3}\eta & \frac{4}{3}\eta & 0 \\ 0 & 0 & \eta \end{bmatrix} \begin{Bmatrix} \partial \dot{u}_x/\partial x \\ \partial \dot{u}_y/\partial y \\ \frac{\partial \dot{u}_x}{\partial y}+\frac{\partial \dot{u}_y}{\partial x} \end{Bmatrix}, \tag{2}$$

where ρ, K, μ, and η are the density, elastic bulk modulus, elastic shear modulus, and dynamic viscosity, respectively; σ_{xx}, σ_{yy}, and σ_{xy} are the two normal components and the shear component of the stress tensor, respectively; and u_x and u_y are the two components of the displacement vector field. One and two dots above the displacements represent the first and second time derivative, respectively.

The governing equations 1 and 2 are discretized in space using the spatial FE method. Triangular isoparametric elements are employed having seven nodes and biquadratic continuous shape functions (Cuvelier et al., 1986). The unstructured triangular mesh is generated by the software triangle (Shewchuck, 2002), which produces high-quality, Delaunay-type meshes. This allows accurately resolving and discretizing the fracture (Frehner and Schmalholz, 2010) without the need of a very fine resolution away from the fracture. Krüger et al. (2005) demonstrate that scattering and diffraction of seismic body waves at a dry fracture may be accurately modeled with a relatively low resolution of the fracture. However, describing the fluid filling the fracture with a more realistic viscoelastic rheology (equation 2) allows for a viscous shear motion in the fluid, which is of a diffusive type. The corresponding diffusion length, L_d, can be calculated as

$$L_d = 2\sqrt{\frac{\eta}{\rho_f}\frac{1}{f_d}}, \tag{3}$$

where ρ_f and f_d are the density of the fluid and the dominant frequency of the incident wave. The triangular mesh used inside the fracture accurately resolves the diffusion length. For example, close to the fracture tip, the minimum node-to-node distance is approximately 50 times smaller than the diffusion length and the total number of elements inside the fracture is approximately 43,000. Such high resolution of the fracture allows for a very accurate modeling of the Krauklis wave motion. At the same time, the maximum node-to-node distance in the surrounding elastic medium far away from the fracture is more than four orders of magnitude larger than inside the fracture, but it still sufficiently resolves the propagating body waves.

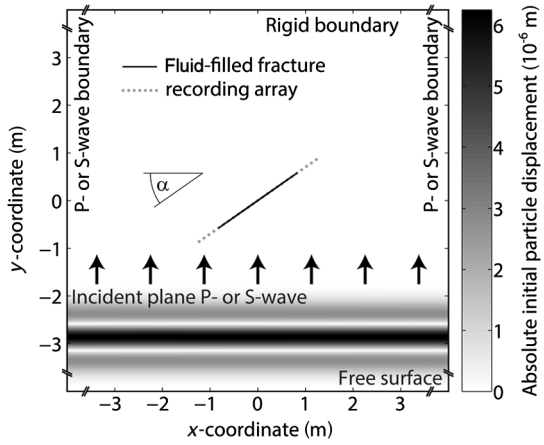

Figure 1. Model setup for studying Krauklis wave initiation by an incident plane body wave. The boundaries are far enough away from the central fracture not have any reflections from the boundaries polluting the analyzed seismograms. Boundary and initial conditions are explained in the text.

The discretization in time is done by an implicit finite-difference scheme (Newmark, 1959; Zienkiewicz and Taylor, 2000). The implicit scheme is unconditionally stable and is therefore favorable over explicit schemes because the time increment can be chosen independently of the extremely fine spatial resolution at the fracture tips (Frehner et al., 2008) and independently of the applied viscosity of the fluid. The standard direct solver provided by MATLAB is used for solving the resulting linear system of equations.

The numerical setup is shown in Figure 1, and the applied material parameters are listed in Table 1. A thin water-filled elliptical fracture with a length of 2 m and an aspect ratio of 333 is embedded in a homogeneous purely elastic surrounding medium. The water in the fracture is viscoelastic, modeled as purely elastic in the bulk (volume) deformation behavior and purely viscous in the deviatoric (shear) deformation behavior. At the fracture walls, there is no relative movement between the water and the surrounding solid (i.e., continuous displacement field across fracture wall). The fracture is inclined with respect to the incident plane body wave by an angle α. The incident plane body (P- or S-) wave's initial particle displacement is the second derivative of a Gaussian (i.e., Ricker wavelet) with a dominant wavelength of $\lambda_d = 1.26$ m. Because the P- and S-wave velocities are different, the dominant frequency of the incident P- and S-wave is different and is $f_d = 1815$ Hz (incident P-wave) and $f_d = 1233$ Hz (incident S-wave). The boundary conditions are a free surface (zero traction) at the bottom, which facilitates initiating the incident plane body wave, and a rigid boundary (zero displacement) at the top. The boundary conditions on the left and right side of the model are chosen depending on the incident wave mode:

- For incident P-wave simulations: P-wave boundary conditions
  The P-wave boundary conditions correspond to an immobile free slip wall, which is defined as zero boundary-parallel

Table 1. Material and model parameters for numerical simulations.

Material parameter	Solid (rock)	Fluid (water)
Elastic bulk modulus K	5 GPa	2.2 GPa
Elastic shear modulus μ	6 GPa	0 Pa
Dynamic viscosity η	0 Pa s	1×10^{-3} Pa s
Density ρ	2500 kg/m^3	1000 kg/m^3
P-wave velocity V_P	2280 m/s	1483 m/s
S-wave velocity V_S	1549 m/s	—
Diffusion length L_d (equation 3)	—	4.7×10^{-3} m (for incident P-wave); 5.7×10^{-3} m (for incident S-wave)
Krauklis wave velocity V_K (Korneev, 2008)	552 m/s (at $f_d = 1815$ Hz for incident P-wave); 495 m/s (at $f_d = 1233$ Hz for incident S-wave)	
Crack stiffness C (Chouet, 1986)	122	
Viscous damping loss F (Chouet, 1986)	2.9×10^{-4}	

shear stress and zero boundary-perpendicular displacement. The plane P-wave can propagate along this boundary without being disturbed.

- For incident S-wave simulations: S-wave boundary conditions
  The S-wave boundary conditions are defined as zero boundary-perpendicular normal stress and zero boundary-parallel displacement. The plane S-wave can propagate along this boundary without being disturbed.

A virtual receiver line running parallel to the long axis of the fracture records the seismic signal (particle displacement). The receiver line is centered in the fracture and therefore also records the seismic signals inside the fracture (Figure 1).

RESULTS

The analysis of the numerical simulations is divided into two parts. First, the wavefield and the recorded seismograms are shown and analyzed. Second, the initiation of Krauklis waves by the passing plane body wave is quantified.

Wavefield and seismograms

Figure 2 shows five snapshots of the simulation with an incident P-wave and an inclination angle of 45°. The theoretical incident P-wavefield is subtracted from the total wavefield. Therefore, only secondary waves (i.e., reflected, scattered, diffracted, and mode-converted) are visible. The predominant secondary waves are body waves, which are reflected and scattered at the fracture and diffracted at the two fracture tips. These secondary body waves produce a complex interference pattern as they radiate away from both fracture tips (e.g., Figure 2d). However, initiated Krauklis waves cannot be identified in Figure 2. Figure 3 shows five snapshots of the simulation with an incident S-wave and an inclination angle of 45°. As in Figure 2, the wavefield of the incident S-wave is subtracted from the total wavefield to enhance the secondary waves. Also in this case, secondary body waves reflected and scattered at the fracture are well visible. In addition, two Krauklis waves are clearly initiated at each of the two fracture tips. They are characterized by high amplitudes close to the fracture, which rapidly decrease away from the fracture. Their slow propagation compared to the body waves is evident by comparing the propagation distance between two snapshots in Figure 3.

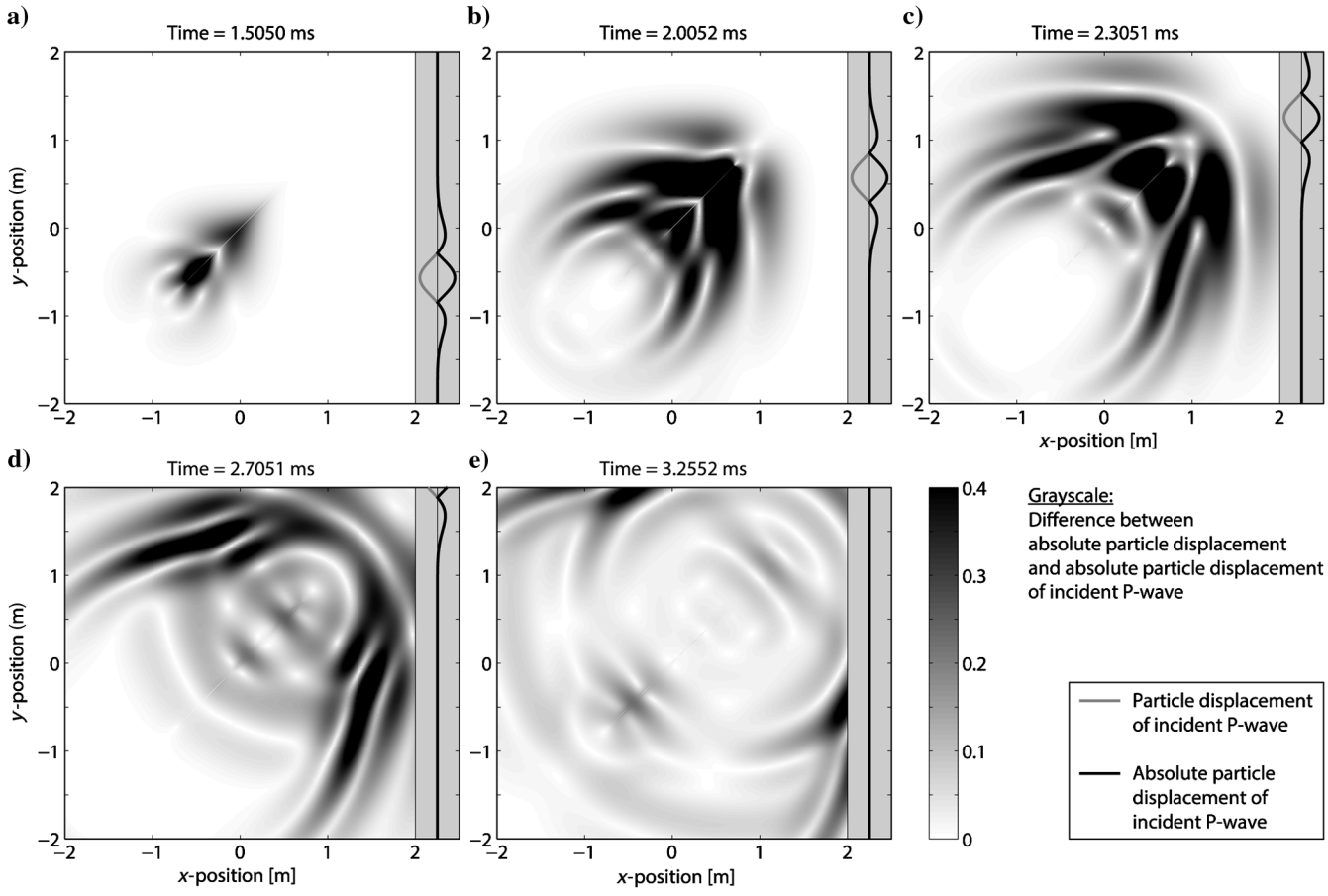

Figure 2. Simulation snapshots of a plane P-wave passing a water-filled fracture with an inclination angle of $\alpha = 45°$. The incident P-wave consisting of a single Ricker wavelet is propagating from the bottom of the model toward the top, and its profile is shown in the gray sidebars of each subfigure. Gray shades display the differential absolute particle displacement of the wavefield (i.e., the difference between the total wavefield and the incident P-wave).

Because the fracture is too thin, Figures 2 and 3 do not conclusively reveal the wavefield inside the fracture. Therefore, Figures 4 and 5 display seismic time sections along the receiver line shown in Figure 1 for different inclination angles α and for incident P- (Figure 4) and S-waves (Figure 5). In both figures, only the fracture-parallel displacement is shown because the Krauklis waves are not visible in the fracture-perpendicular direction. As in the previous snapshots (Figures 2 and 3), the wavefield of the incident body wave is subtracted from the total wavefield to highlight the secondary waves. In all seismic sections in Figures 4 and 5, only the incident body wave and two Krauklis waves can be identified. All other possible wave types are not initiated. A similar observation is made by Derov et al. (2008) and Maksimov et al. (2011), who also only identify the incident and the Krauklis wave. This indicates that the Krauklis wave is indeed the predominant wave mode in fractures, as Korneev (2010) suggests.

For incident P-waves, the largest Krauklis wave amplitudes are initiated for an inclination angle of 75° (Figure 4c) and the smallest for an inclination angle of 45° (Figure 4b). This is also the reason why the Krauklis wave cannot be identified in Figure 2. In the case of an incident S-wave, the largest Krauklis wave amplitudes are initiated at a 45° inclination angle (Figure 5b), whereas the other inclination angles show smaller Krauklis wave amplitudes. In all cases, two Krauklis waves are initiated by the incident body wave, one at each fracture tip, which corresponds to the two diffraction points of the fracture. For P- and S-wave incidence, the two initiated Krauklis waves exhibit opposite polarity, which can be best seen at low inclination angles (Figures 4a and 5a). From the slope in the seismic sections, it is evident that the Krauklis waves propagate along the fracture with a very low velocity (Table 1). The strong dispersion of the Krauklis waves can also be observed in Figures 4 and 5. The group velocity is considerably higher than the phase velocity, whereas the latter is well predicted by the analytical value. In other words, the envelope of the Krauklis wave signal propagates faster than the individual peaks and troughs. The strong dispersion also leads to a stretching of the Krauklis wave signal with increasing propagation distance (i.e., toward the bottom of each panel in Figures 4 and 5).

Initiated Krauklis wave amplitude

Close to the fracture tips, the Krauklis waves interfere with the incident body wave (Figures 4 and 5). However, in the central part of the fracture, it is straightforward to isolate the Krauklis waves because they are the only initiated secondary waves and have a distinctively different propagation velocity compared to the incident wave. Figures 6 (incident P-wave) and 7 (incident S-wave) display the amplitude of the initiated Krauklis waves along the central part of the fracture for all possible inclination angles. For both incident wave modes, a distinct interference pattern occurs when the two

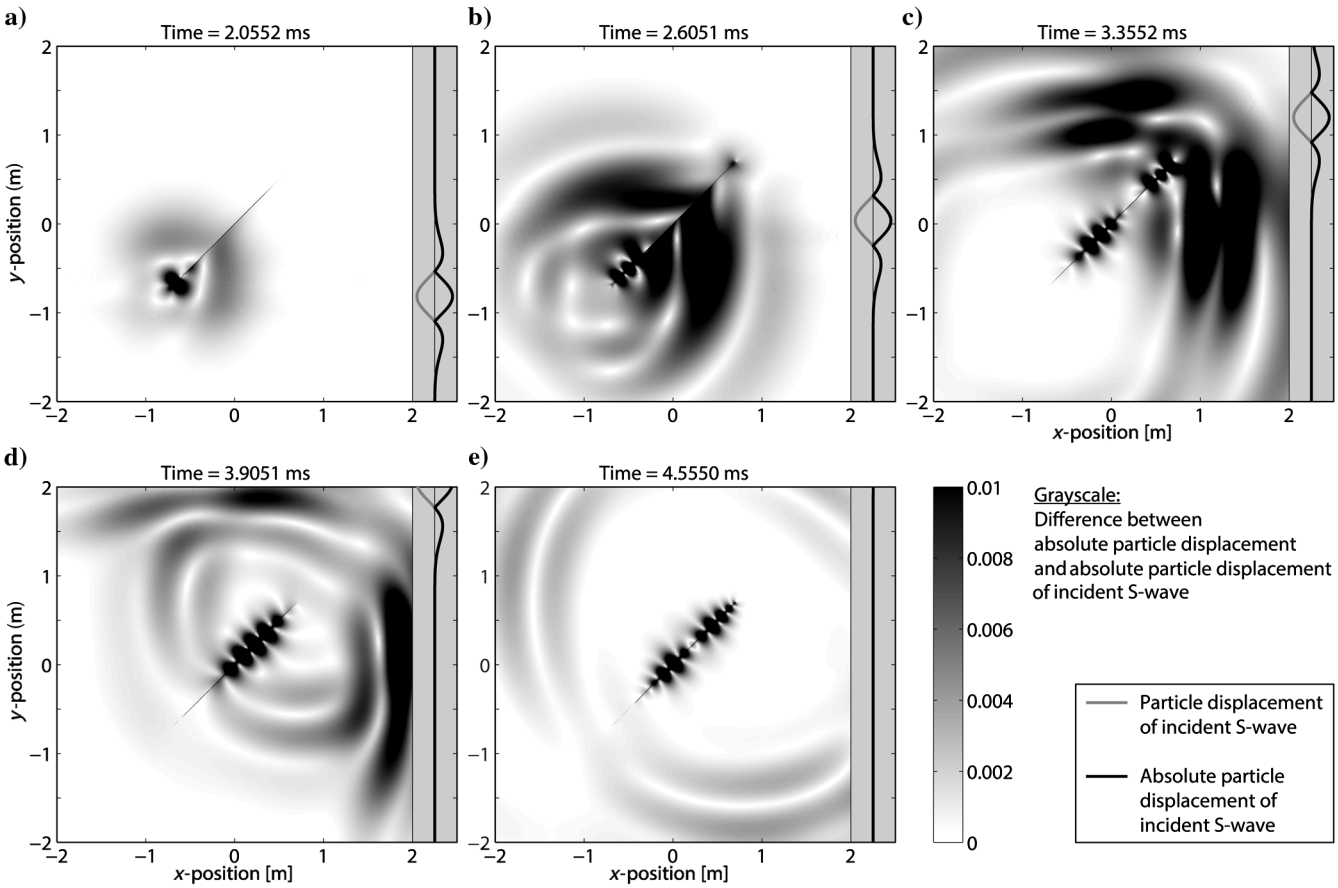

Figure 3. Same as Figure 2, but for an incident S-wave. Note the different grayscale values compared to Figure 2.

initiated Krauklis waves pass each other (Figures 6a and 7a). It consists of a central low, which is due to the opposite polarity of the two interfering Krauklis waves, flanked by two high-amplitude values. Because of the strong Krauklis wave dispersion, this interference pattern occurs slightly on the far side of the intersection between the theoretical Krauklis wave phase velocities drawn from the two fracture tips (white line in Figures 6a and 7a).

In the case of an incident P-wave, Figure 6 demonstrates that the initiation of Krauklis waves strongly depends on the fracture orientation. Large amplitude Krauklis waves are initiated for inclination angles of the fracture α between 12° and 40° or larger than 65°. For inclination angles smaller than approximately 12° and between approximately 40° and 65°, the mean Krauklis wave amplitude (Figure 6b) is more than one order of magnitude smaller than the incident P-wave amplitude and can therefore be considered negligible for these angles. The largest-amplitude Krauklis waves are initiated when the propagation direction of the P-wave is parallel to the fracture (i.e., $\alpha = 90°$).

In the case of an incident S-wave, Figure 7 shows an equally strong dependency of the initiated Krauklis wave amplitude on the fracture orientation. However, there are two major differences to the incident P-wave case. First, the initiated Krauklis waves generally have considerably larger mean amplitude for all inclination angles smaller than 80° (Figure 7b). Within this angular range, large-amplitude Krauklis waves are initiated by the incident S-wave and must be considered significant. Second, the dependency of the initiated Krauklis wave amplitude on fracture orientation for the incident S-wave case (Figure 7) is almost inverse to that in the case of an incident P-wave (Figure 6). For example, the largest-amplitude Krauklis waves are initiated at an inclination angle of approximately 50° (Figure 7), which is the inclination angle with the smallest-amplitude Krauklis waves in the case of an incident P-wave (Figure 6).

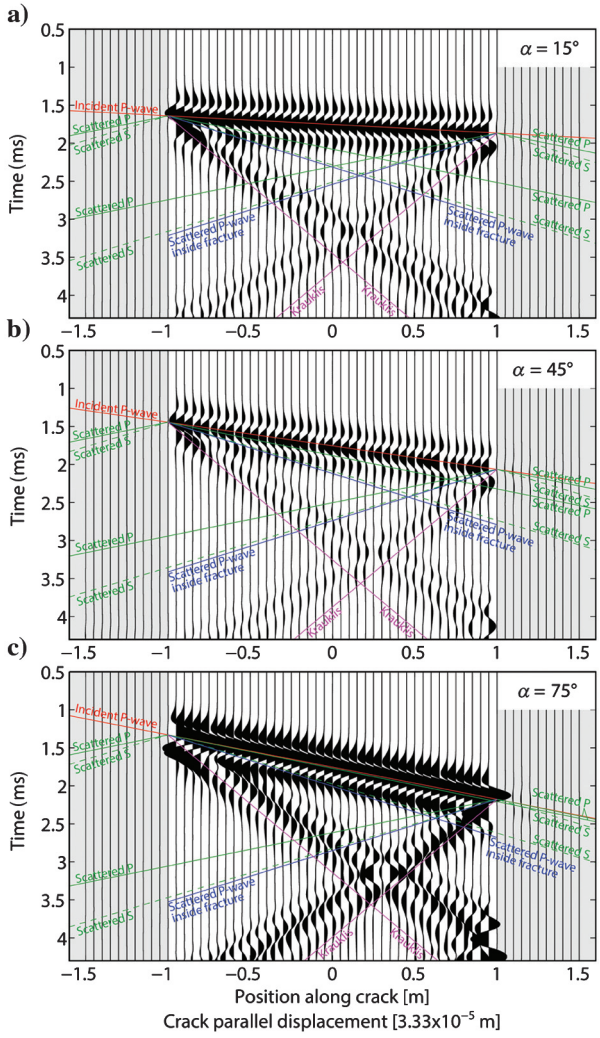

Figure 4. Seismic time sections of the receiver line passing through the center of the fracture (Figure 1) displaying the fracture-parallel component of the differential particle displacement (i.e., difference between total wavefield and incident P-wave). Subfigures (a-c) show results for different inclination angles, $\alpha = [15°, 45°, 75°]$. Straight lines depict theoretical phase velocities of different wave modes for the particular frequency of 1815 Hz. Gray shaded areas correspond to receivers outside the fracture; the white central area corresponds to receivers within the fracture.

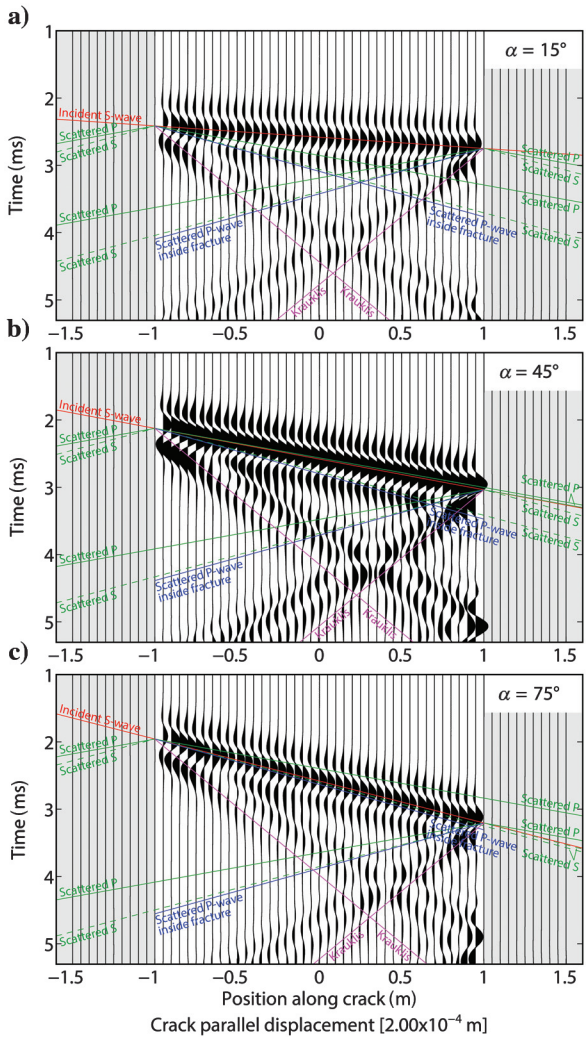

Figure 5. Same as Figure 4, but for an incident S-wave and a frequency of 1233 Hz. Note the different amplitude scale compared to Figure 4.

DISCUSSION

Both incident P- and S-waves are capable of initiating Krauklis waves at the two fracture tips. In the studied case of a single smooth fracture, the initiation points correspond to the two diffraction points of the fracture. Real fractures may have rough surfaces or different fracture sets may intersect each other, which leads to more diffraction points along a fracture in natural rocks. The case of intersecting fractures may be comparable to a fracture intersecting a borehole, for which it is well known that Krauklis waves are initiated at the intersection point (e.g., Ionov, 2007; Maksimov et al., 2011). Therefore, it can be expected that the potential for Krauklis wave initiation of a body wave passing through a natural fractured rock is much higher than in the studied simplified case. S-waves initiate significantly larger-amplitude Krauklis waves than P-waves. Therefore, it is expected that S-waves propagating through fractured fluid-saturated reservoir rocks carry more information about the fractures (for example, fracture density, orientation, or fluid content) than P-waves.

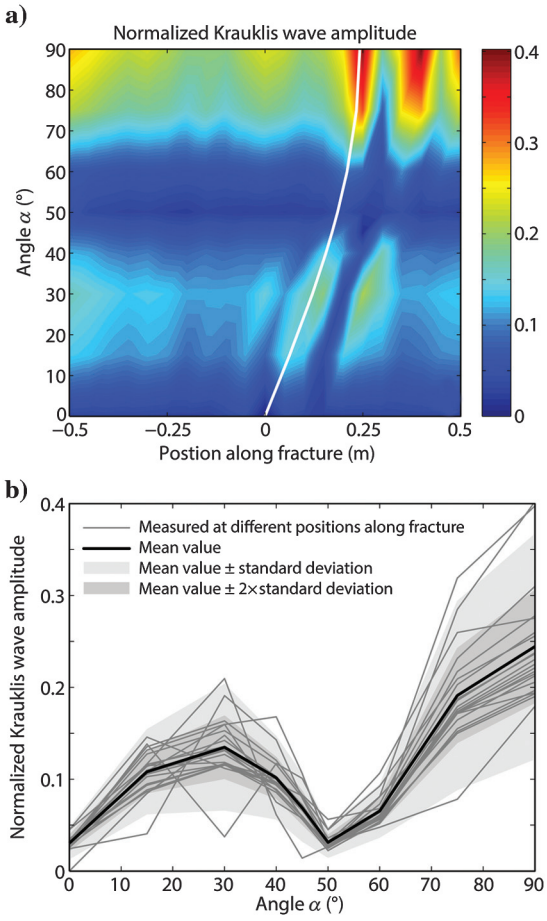

Figure 6. (a) Krauklis wave amplitude in the fracture-parallel direction, normalized by the incident P-wave amplitude, as a function of the recording position along the fracture and the inclination angle of the fracture α. The white line corresponds to the location where the analytical Krauklis wave phase velocities drawn from the two fracture tips cross each other (Figure 4). (b) All recordings of (a) along the fracture plotted on top of each other as a function of inclination angle α together with the mean value and standard deviation.

It is more intuitive that Krauklis waves can be initiated by a seismic source within the fracture (Chouet, 1986; Frehner and Schmalholz, 2010). Such sources may represent fracture opening or propagation events due to fluid migration, for example, in volcanic areas (Chouet, 1986), or due to hydrofracturing of a hydrocarbon reservoir. However, Krauklis wave initiation by a body wave propagating through a fractured fluid reservoir has some severe implications. For example, seismic earthquake signals may initiate Krauklis waves in volcanic areas, where magmatic dykes and sills act as waveguides, or active exploration seismic sources may excite Krauklis waves in fractured hydrocarbon or geothermal reservoirs. Because the Krauklis wave initiation is a function of the fracture orientation (Figures 6 and 7), the modified body waves propagating through a fractured fluid-saturated rock are expected to carry information about the fracture orientation. In particular, the combined analysis of P- and S-waves should help extract this information from seismic signals because their sensitivity to fracture orientation is quite different (Figures 6 and 7). It is the aim of future studies to develop strategies for extracting fracture orientation-information from seismic recordings.

The present study only considers incident body waves with a given wavelength (1.26 m). Because the initiated Krauklis waves are strongly dispersive (Korneev, 2008), the initiation process is expected to be frequency dependent and the presented results may not

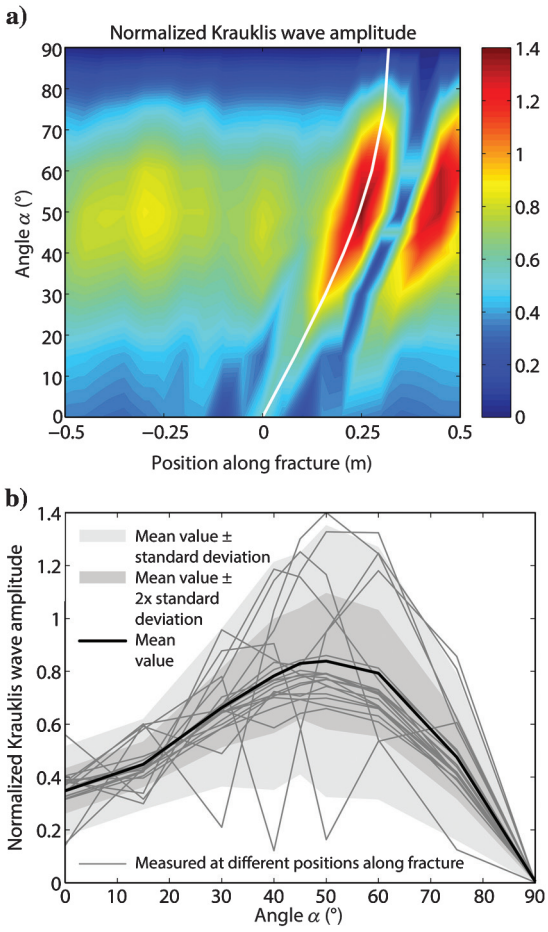

Figure 7. Same as Figure 6, but for an incident S-wave. Note the different color scale values in (a) compared to Figure 6.

be generalized to frequencies much different than the used ones. Derov et al. (2008) and Maksimov et al. (2011) observe that Krauklis waves are also initiated with large amplitude at a frequency of 700 Hz, which is roughly half the frequency used here. However, the Krauklis wave initiation at frequencies much larger (e.g., MHz range) or much smaller (e.g., 1 Hz range) still remains to be studied in future investigations.

Once initiated, Krauklis waves can propagate back and forth along a fracture several times. The repeated back-and-forth propagation corresponds to a rock-internal oscillatory behavior. Each time the Krauklis wave reaches a fracture tip or an intersection with another fracture, part of the Krauklis wave is mode-converted into body waves and emitted into the surrounding rock (Frehner and Schmalholz, 2010). Therefore, Krauklis wave-related seismic signals may also be detected further away from the fractures. The interaction between seismic body-wave propagation and rock-internal oscillatory behavior has been studied by Frehner et al. (2009, 2010), Huang et al. (2009), and Steeb et al. (2010, 2012). If the oscillatory behavior can be described by a narrow distribution of resonance frequencies, the body waves exhibit a strong dispersion. Therefore, Krauklis wave effects in a rock with a narrow distribution of fracture lengths should lead to a strongly frequency-dependent wave propagation behavior for body waves, as Korneev (2008) speculates. On the other hand, if the resonance frequencies are widely distributed, the model of Steeb et al. (2012) predicts that the rock's dispersion behavior stays the same, but the peak dispersion and attenuation are shifted to higher frequencies. Therefore, Krauklis wave effects in a rock with strongly varying fracture lengths should not lead to such a pronounced frequency dependency for body-wave propagation, but the dependency on fracture orientation may still remain.

The above-mentioned effective medium models (Frehner et al., 2009, 2010; Huang et al., 2009; Steeb et al., 2010, 2012), incorporating a rock-internal oscillatory behavior into wave propagation models, are isotropic. However, Figures 6 and 7 demonstrate that Krauklis wave initiation strongly depends on fracture orientation, reflecting an anisotropy effect. Such effects need to be considered in the future when developing effective medium theories for fractured rocks.

The presented study is based on a 2D (plane strain) problem description assuming an infinite model extension in the out-of-plane dimension. Therefore, the results and interpretations are valid for fractures substantially elongated in this third direction, such as oblate or penny-shaped fractures. For fractures with a more prolate (cigar) shape, fully 3D numerical simulations are necessary and the results and interpretations may slightly deviate from the presented ones.

CONCLUSIONS

Seismic body waves propagating through a fractured fluid-filled rock can initiate Krauklis waves of significant amplitude. The initiation strongly depends on the incident wave mode (P- or S-wave) and fracture orientation. Generally, S-waves initiate significantly larger-amplitude Krauklis waves than P-waves, and S-waves are therefore expected to carry more information about the fractures. In the case of an incident P-wave, almost no Krauklis waves are initiated for small inclination angles and for inclination angles between 40° and 65°; the strongest initiation occurs when the P-wave propagates parallel to the length of the fracture. In the case of an incident S-wave, the dependency of Krauklis wave initiation on fracture orientation is almost inverse to the case of an incident P-wave; the largest-amplitude Krauklis waves are initiated at an inclination angle of approximately 50°. Initiating Krauklis waves should lead to a strongly frequency-dependent and anisotropic propagation behavior for body waves, particularly in the case of a single fracture set with constant orientation and length.

ACKNOWLEDGMENTS

This work resulted from the project UPseis, supported by the Swiss National Science Foundation, Project no. 200021_143319. E. H. Saenger, B. Quintal, and P.-J. Shih are acknowledged for countless stimulating discussions.

REFERENCES

Aki, K., M. Fehler, and S. Das, 1977, Source mechanism of volcanic tremor: Fluid-driven crack models and their application to the 1963 Kilauea eruption: Journal of Volcanology and Geothermal Research, **2**, 259–287, doi: 10.1016/0377-0273(77)90003-8.

Ashour, A. S., 2000, Wave motion in a viscous fluid-filled fracture: International Journal of Engineering Science, **38**, 505–515, doi: 10.1016/S0020-7225(99)00045-2.

Biot, M. A., 1962, Mechanics of deformation and acoustic propagation in porous media: Journal of Applied Physics, **33**, 1482–1498, doi: 10.1063/1.1728759.

Bourbie, T., O. Coussy, and B. Zinszner, 1987, Acoustics of porous media: Editions Technip.

Carcione, J. M., 2001, Wave fields in real media: Wave propagation in anisotropic, anelastic and porous media: Elsevier.

Carcione, J. M., and H. B. Helle, 2004, The physics and simulation of wave propagation at the ocean bottom: Geophysics, **69**, 825–839, doi: 10.1190/1.1759469.

Chouet, B., 1986, Dynamics of a fluid-driven crack in three dimensions by the finite-difference method: Journal of Geophysical Research, **91**, 13967–13992, doi: 10.1029/JB091iB14p13967.

Chouet, B., 1988, Resonance of a fluid-driven crack: Radiation properties and implications for the source of long-period events and harmonic tremor: Journal of Geophysical Research, **93**, 4375–4400, doi: 10.1029/JB093iB05p04375.

Chouet, B., 1996, Long-period volcano seismicity: Its source and use in eruption forecasting: Nature, **380**, 309–316, doi: 10.1038/380309a0.

Cuvelier, C., A. Segal, and A. A. von Steenhoven, 1986, Finite element methods and Navier-Stokes equations: D. Reidel Publishing Company.

Derov, A. V., G. A. Maximov, and M. Y. Lazarkov, 2008, On boundary condition at tips of fluid filled fracture for description of the slow fracture mode generation by external acoustical field the effective boundary condition of the mixed, *in* O. V. Rudenko, A. V. Korchak, and S. N. Gurbatov, Proceedings of the XX Session of the Russian Acoustical Society: Russian Acoustical Society, 184–186.

Dvorkin, J., G. Mavko, and A. Nur, 1995, Squirt flow in fully saturated rocks: Geophysics, **60**, 97–107, doi: 10.1190/1.1443767.

Ferrazzini, V., and K. Aki, 1987, Slow waves trapped in a fluid-filled infinite crack: Implication for volcanic tremor: Journal of Geophysical Research, **92**, 9215–9223, doi: 10.1029/JB092iB09p09215.

Ferrazzini, V., B. Chouet, M. Fehler, and K. Aki, 1990, Quantitative-analysis of long-period events recorded during hydrofracture experiments at Fenton Hill, New Mexico: Journal of Geophysical Research, **95**, 21871–21884, doi: 10.1029/JB095iB13p21871.

Frehner, M., 2013, Krauklis wave initiation in fluid-filled fractures by a passing body wave, *in* C. Hellmich, B. B. Pichler, and D. Adam, eds., Poromechanics V: Proceedings of the fifth Biot Conference on Poromechanics: American Society of Civil Engineers, 92–100.

Frehner, M., and S. M. Schmalholz, 2010, Finite-element simulations of Stoneley guided-wave reflection and scattering at the tips of fluid-filled fractures: Geophysics, **75**, no. 2, T23–T36, doi: 10.1190/1.3340361.

Frehner, M., S. M. Schmalholz, and Y. Podladchikov, 2009, Spectral modification of seismic waves propagating through solids exhibiting a resonance frequency: A 1-D coupled wave propagation-oscillation model: Geophysical Journal International, **176**, 589–600, doi: 10.1111/j.1365-246X.2008.04001.x.

Frehner, M., S. M. Schmalholz, E. H. Saenger, and H. Steeb, 2008, Comparison of finite difference and finite element methods for simulating two-dimensional scattering of elastic waves: Physics of the Earth and Planetary Interiors, **171**, 112–121, doi: 10.1016/j.pepi.2008.07.003.

Frehner, M., H. Steeb, and S. M. Schmalholz, 2010, Wave velocity dispersion and attenuation in media exhibiting internal oscillations, *in* A. Petrin, ed., Wave propagation in materials for modern applications: In-Tech Education and Publishing, 455–476.

Groenenboom, J., and J. Falk, 2000, Scattering by hydraulic fractures: Finite-difference modeling and laboratory data: Geophysics, **65**, 612–622, doi: 10.1190/1.1444757.

Groenenboom, J., and D. B. van Dam, 2000, Monitoring hydraulic fracture growth: Laboratory experiments: Geophysics, **65**, 603–611, doi: 10.1190/1.1444756.

Huang, H. H., C. T. Sun, and G. L. Huang, 2009, On the negative effective mass density in acoustic metamaterials: International Journal of Engineering Science, **47**, 610–617, doi: 10.1016/j.ijengsci.2008.12.007.

Ionov, A. M., 2007, Stoneley wave generation by an incident P-wave propagating in the surrounding formation across a horizontal fluid-filled fracture: Geophysical Prospecting, **55**, 71–82, doi: 10.1111/j.1365-2478.2006.00577.x.

Korneev, V., 2008, Slow waves in fractures filled with viscous fluid: Geophysics, **73**, no. 1, N1–N7, doi: 10.1190/1.2802174.

Korneev, V., 2010, Low-frequency fluid waves in fractures and pipes: Geophysics, **75**, no. 6, N97–N107, doi: 10.1190/1.3484155.

Korneev, V., 2011, Krauklis wave in a stack of alternating fluid-elastic layers: Geophysics, **76**, no. 6, N47–N53, doi: 10.1190/geo2011-0086.1.

Korneev, V., G. Goloshubin, B. Kashtan, A. Bakulin, V. Troyan, G. Maximov, L. Molotkov, M. Frehner, S. Shapiro, and R. Shigapov, 2012, Krauklis wave — Half a century after: 74th Annual International Conference and Exhibition, EAGE, Extended Abstracts, B008.

Korneev, V. A., A. A. Ponomarenko, and M. Kashtan, 2009, Stoneley guided waves: What is missing in Biot's theory?, *in* H. I. Ling, A. Smyth, and R. Betti, eds., Poromechanics IV: Proceedings of the fourth Biot conference on poromechanics: DEStech Publications Inc., 706–711.

Krauklis, P. V., 1962, About some low frequency oscillations of a liquid layer in elastic medium: Prikladnaya Matematika i Mekhanika, **26**, 1111–1115.

Krüger, O. S., E. H. Saenger, and S. A. Shapiro, 2005, Scattering and diffraction by a single crack: An accuracy analysis of the rotated staggered grid: Geophysical Journal International, **162**, 25–31, doi: 10.1111/j.1365-246X.2005.02647.x.

Lambert, M.-A., E. H. Saenger, B. Quintal, and S. M. Schmalholz, 2013, Numerical simulation of ambient seismic wavefield modification caused by pore-fluid effects in an oil reservoir: Geophysics, **78**, no. 1, T41–T52, doi: 10.1190/geo2011-0513.1.

Lloyd, P., and M. Redwood, 1965, Wave propagation in a layered plate composed of two solids with perfect contact, slip, or a fluid layer at their interface: Acustica, **16**, 224–232.

Maksimov, G. A., A. V. Derov, B. M. Kashtan, and M. Y. Lazarkov, 2011, Estimation of hydro-fracture parameters by analysis of tube waves at vertical seismic profiling: Acoustical Physics, **57**, 529–541, doi: 10.1134/S1063771011040166.

Mavko, G., and D. Jizba, 1991, Estimating grain-scale fluid effects on velocity dispersion in rocks: Geophysics, **56**, 1940–1949, doi: 10.1190/1.1443005.

Newmark, N. M., 1959, A method of computation for structural dynamics: Journal of the Engineering Mechanics Division, **85**, 67–94.

Paillet, F. L., and J. E. White, 1982, Acoustic modes of propagation in the borehole and their relationship to rock properties: Geophysics, **47**, 1215–1228, doi: 10.1190/1.1441384.

Quintal, B., H. Steeb, M. Frehner, and S. M. Schmalholz, 2011, Quasi-static finite element modeling of seismic attenuation and dispersion due to wave-induced fluid flow in poroelastic media: Journal of Geophysical Research, **116**, B01201, doi: 10.1029/2010JB007475.

Scholte, J. G., 1942a, On the Stoneley-wave equation I: Proceedings of the Koninklijke Nederlandse Akademie van Wetenschappen, **45**, 20–25.

Scholte, J. G., 1942b, On the Stoneley-wave equation II: Proceedings of the Koninklijke Nederlandse Akademie van Wetenschappen, **45**, 159–164.

Shewchuck, J. R., 2002, Delaunay refinement algorithms for triangular mesh generation: Computational Geometry, **22**, 21–74, doi: 10.1016/S0925-7721(01)00047-5.

Steeb, H., M. Frehner, and S. M. Schmalholz, 2010, Waves in residual-saturated porous media, *in* G. A. Maugin, and A. V. Metrikine, eds., Mechanics of generalized continua: One hundred years after the Cosserats: Springer Verlag, vol. 17, 9–190.

Steeb, H., P. Kurzeja, M. Frehner, and S. M. Schmalholz, 2012, Phase velocity dispersion and attenuation of seismic waves due to trapped fluids in residual saturated porous media: Vadose Zone Journal, **11**, doi: 10.2136/vzj2011.0121.

Stoneley, R., 1924, Elastic waves at the surface of separation of two solids: Proceedings of the Royal Society of London, Series A, **106**, 416–428, doi: 10.1098/rspa.1924.0079.

White, J. E., 1975, Computed seismic speeds and attenuation in rocks with partial gas saturation: Geophysics, **40**, 224–232, doi: 10.1190/1.1440520.

White, J. E., N. G. Mikhaylova, and F. M. Lyakhovitsky, 1975, Low-frequency seismic-waves in fluid-saturated layered rocks: Physics of the Solid Earth, **11**, 654–659, doi: 10.1121/1.995164.

Yamamoto, M., and H. Kawakatsu, 2008, An efficient method to compute the dynamic response of a fluid-filled crack: Geophysical Journal International, **174**, 1174–1186, doi: 10.1111/j.1365-246X.2008.03871.x.

Zienkiewicz, O. C., and R. L. Taylor, 2000, The finite element method: Its basis and fundamentals, **1**, 5th ed.: Butterworth-Heinemann.